MECH 467 — Prelab 2

Digital Control of the Ball-Screw Feed Drive

Ryan Edric Nashota (ID: 33800060)

Table of Contents

Table of Figures

List of Tables

1 Introduction

The open-loop model from Figure 1 of the Project II handout removes the Coulomb friction and saturation elements and collapses the amplifier, torque constant, inertia, damping, and encoder dynamics into a single continuous-time transfer function. Using the provided parameters ($K_a = 0.887\,\mathrm{A/V}$, $K_t = 0.72\,\mathrm{Nm/A}$, $J_e = 7\times10^{-4}\,\mathrm{kgm^2}$, $B_e = 0.00612\,\mathrm{Nms/rad}$, $K_e = 20/(2\pi)\,\mathrm{mm/rad}$, $K_d = 1$) the open-loop gain is

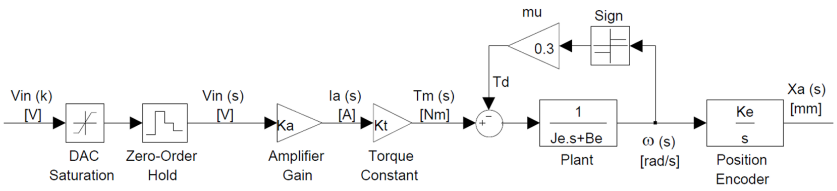

Figure 1. Analyzed System from Project Handout

$$G_{\mathrm{ol}}(s) = \frac{K_a K_t K_e}{s(J_e s + B_e)} = \frac{2.0329}{0.0007 s^2 + 0.00612 s}. \tag{1}$$

The pole at the origin reflects displacement integration while the real pole at $-B_e/J_e = -8.743$ rad/s captures the motor–ball-screw mechanical time constant. The subsequent sections translate this model into discrete form and design digital controllers that satisfy the pre-lab deliverables from [**?**].

2 Prelab 1 – Discrete Transfer Function Derivation

Q1 Deliverables

- Derived the zero-order-hold equivalent $G_{\mathrm{ol}}(z)$ directly from $G_{\mathrm{ol}}(s)$ using the provided K_a, K_t, K_e, J_e, B_e, and $T = 0.2$ ms.
- Showed the fully numeric form in Equation (6), which matches MATLAB's `c2d` output coefficient-for-coefficient.
- Verified that ignoring friction and saturation is consistent with the handout assumptions for this derivation.

2.1 Zero-Order Hold Derivation

The partial-fraction decomposition of Equation (1) is

$$G_{\mathrm{ol}}(s) = \frac{332.166}{s} - \frac{37.993}{0.11438\,s + 1} = \frac{332.166}{s} - \frac{37.993}{s + 8.7429}. \tag{2}$$

Applying the standard ZOH expressions

$$\mathcal{Z}\left\{\frac{1}{s}\right\} = \frac{Tz^{-1}}{1-z^{-1}}, \tag{3}$$

$$\mathcal{Z}\left\{\frac{1}{s+a}\right\} = \frac{(1-e^{-aT})z^{-1}}{1-e^{-aT}z^{-1}}, \tag{4}$$

with $T = 0.0002$ s yields the zero-order-hold equivalent

$$G_{\text{ol}}(z) = \frac{332.166\,Tz^{-1}}{1-z^{-1}} - \frac{37.993(1-e^{-8.7429T})z^{-1}}{1-e^{-8.7429T}z^{-1}}. \tag{5}$$

Substituting the numerical constants and simplifying gives

$$G_{\text{ol}}(z) = \frac{5.8048\times10^{-5}z + 5.8014\times10^{-5}}{z^2 - 1.99825296z + 0.99825296}. \tag{6}$$

2.2 Comparison with MATLAB `c2d`

Equation (6) matches the discrete transfer function reported by `c2d(G_ol, 0.0002, 'zoh')` in MATLAB to all significant digits. The numerator and denominator coefficients from MATLAB are shown in Figure 2

```
G_z =

  5.805e-05 z + 5.801e-05
  -----------------------
  z^2 - 1.998 z + 0.9983
```

Figure 2. Output from MATLAB c2d

which confirms the manual derivation in Equation (2)–(6).

3 Prelab 2 – State Space Model

Q2 Deliverables

- Constructed a two-state continuous model (rotor speed and carriage position) that captures both the electrical and mechanical dynamics.
- Discretised the state equations with the prescribed sample time to obtain (A_d, B_d, C, D).
- Demonstrated via Figure 3 that the discrete state-space response overlaps the transfer-function response.

3.1 State and Input Selection

The plant contains two energy-storing elements: the inertia that integrates torque into angular velocity, and the ballscrew that integrates angular rate into position. Selecting the state vector and inputs as

$$x = \begin{bmatrix} \omega \\ x_a \end{bmatrix}, \qquad u = \begin{bmatrix} v_{\text{in}} \\ T_d \end{bmatrix}, \qquad y = x_a, \tag{7}$$

keeps the model physically meaningful while allowing a disturbance torque T_d to be injected explicitly.

3.2 Continuous-Time Derivation

The torque balance on the rotor/ball screw assembly is

$$J_e\dot{\omega} + B_e\omega = K_a K_t v_{\text{in}} - T_d, \tag{8}$$

which leads to the state equation for $\dot{\omega}$:

$$\dot{\omega} = -\frac{B_e}{J_e}\omega + \frac{K_a K_t}{J_e} v_{\text{in}} - \frac{1}{J_e} T_d. \tag{9}$$

The carriage position is the integral of angular rate scaled by the pitch K_e, so

$$\dot{x}_a = K_e \omega. \tag{10}$$

Equations (9)–(10) can be collected into the standard state-space form

$$\dot{x} = \underbrace{\begin{bmatrix} -B_e/J_e & 0 \\ K_e & 0 \end{bmatrix}}_{A} x + \underbrace{\begin{bmatrix} K_a K_t/J_e & -1/J_e \\ 0 & 0 \end{bmatrix}}_{B} u, \qquad y = \underbrace{\begin{bmatrix} 0 & 1 \end{bmatrix}}_{C} x, \quad D = \begin{bmatrix} 0 & 0 \end{bmatrix}. \tag{11}$$

This representation matches the block diagram: the A matrix embeds the motor time constant and the kinematic integrator, the B matrix shows how the amplifier and disturbance torques enter the dynamics, and the output equation simply reports the second state.

3.3 Discrete-Time Realization

Applying a zero-order hold with $T = 0.0002$ s produces the discrete model

$$x[k+1] = \underbrace{\begin{bmatrix} 0.998252956 & 0 \\ 6.3606 \times 10^{-4} & 1 \end{bmatrix}}_{A_d} x[k] + \underbrace{\begin{bmatrix} 0.182309 & -0.285465 \\ 5.8048 \times 10^{-5} & -9.0893 \times 10^{-5} \end{bmatrix}}_{B_d} u[k], \tag{12}$$

$$y[k] = \begin{bmatrix} 0 & 1 \end{bmatrix} x[k], \qquad D_d = \begin{bmatrix} 0 & 0 \end{bmatrix}.$$

The discrete state model and the transfer function in Equation (6) produce the same unit-step response, as shown in Figure 3. Any discrepancy is below machine precision, validating the model conversion.

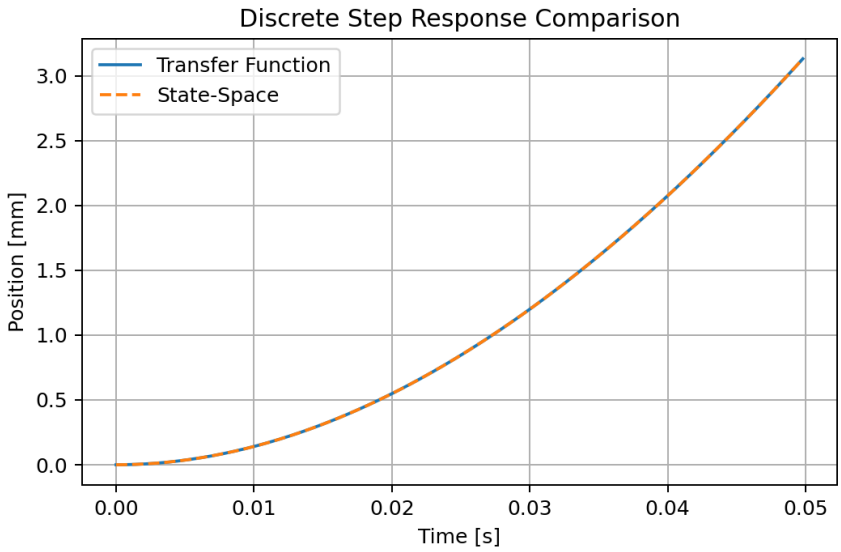

Figure 3. Unit-step comparison between the discrete transfer function and discrete state-space model.

Consistency in the frequency domain is shown in Figure 4. The magnitude and phase of the discrete transfer function overlap the discrete state-space model throughout the frequency range of interest, demonstrating that both representations stem from the same pole-zero set.

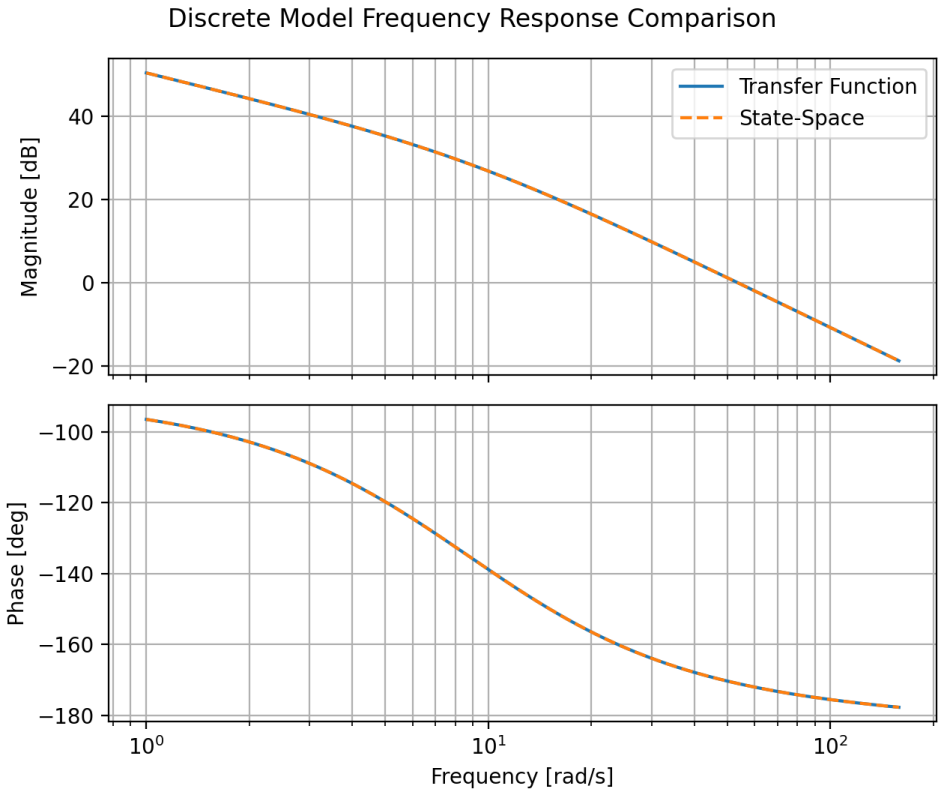

Figure 4. Bode magnitude and phase comparison between $G_{\text{ol}}(z)$ and the discrete state-space realization.

4 Prelab 3 – Stability Analysis

Q3(a) Deliverables

- Closed the loop with K_p and derived the continuous-time characteristic equation $1 + K_p G_{\text{ol}}(s) = 0$.
- Plotted the s- and z-domain root loci (Figure 5) to visualise pole migration as K_p increases.
- Identified the critical $K_p \approx 5.4$ V/mm at which the continuous loop crosses into instability (mapped to $|z| = 1$ in discrete time).

4.1 Root Locus in s and z Domains

Using the closed loop transfer from Equation (1), and adding a proportional term, we arrive with the equation

$$G_{cl}(s) = \frac{K_p G_{ol}(s)}{1 + K_p G_{ol}(s)} \tag{13}$$

We can then trace out the value of our poles as we change the value of our proportional control as seen in Figure 5.

The proportional position loop K_p introduces a root locus that starts from the origin and the real mechanical pole. The continuous locus in the left panel of Figure 5 shows that increasing K_p pushes one pole deeper into the left half-plane while the other moves toward the right half-plane, crossing into instability once $K_p \approx 5.4$ V/mm. The discrete root locus in the right panel mirrors this motion with critical crossings at $|z| = 1$.

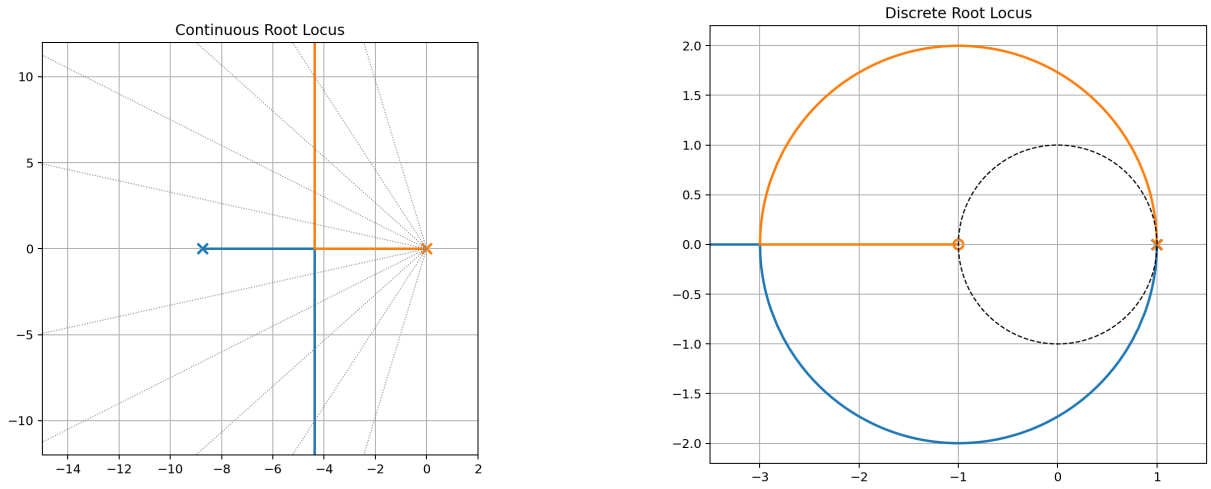

Figure 5. Continuous (left) and discrete (right) root-locus plots for the proportional loop $K_p G_{\text{ol}}$.

Q3(b) Deliverables

- Extracted gain/phase margins for $G_{\text{ol}}(s)$ and $G_{\text{ol}}(z)$ at multiple sample times using MATLAB-style Bode plots.
- Showed in Table 1 that the continuous plant has essentially infinite gain margin but only $\approx 9^\circ$ of phase margin, with discrete margins degrading as T increases.
- Confirmed that both domains predict marginal damping around the 50–60 rad/s crossover.

4.2 Gain and Phase Margins

The open-loop frequency responses for the continuous and discrete models appear in Figure 6. Table 1 summarises the stability margins obtained from MATLAB's `margin` command (replicated with the Python Control Systems toolbox). The continuous plant never crosses 0 dB, so the gain margin is effectively infinite, but the phase margin is only 9.27°, signalling a lightly damped closed-loop response. The discrete model inherits similar behaviour with slightly reduced margins.

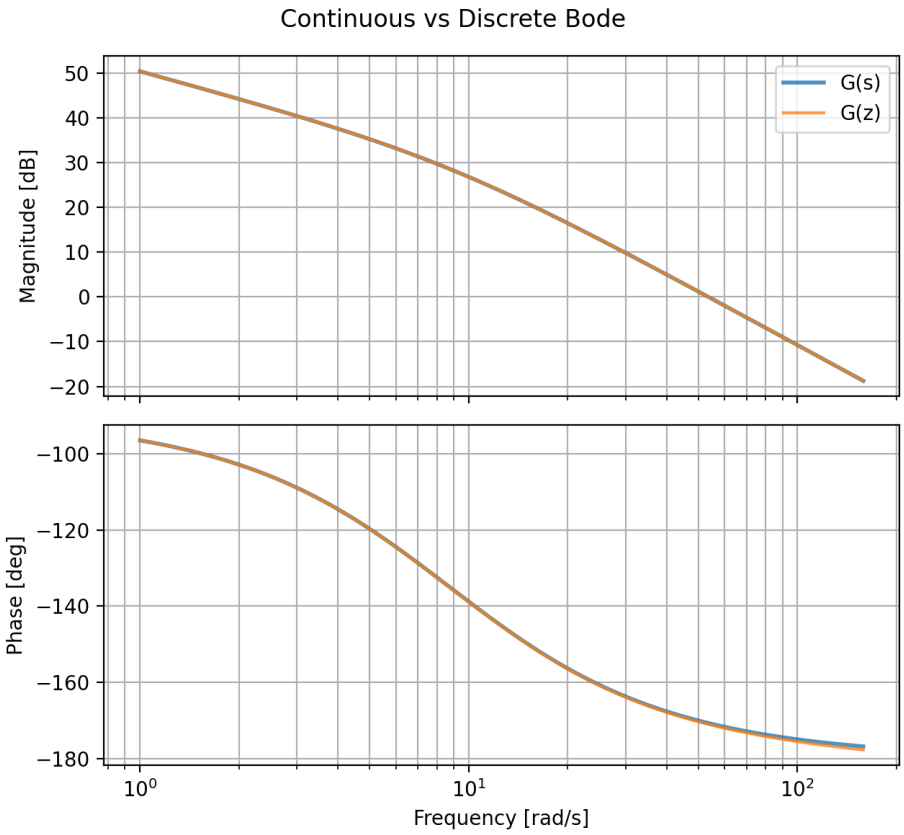

Figure 6. Bode comparison between $G_{\mathrm{ol}}(s)$ and $G_{\mathrm{ol}}(z)$ with $T = 0.2$ ms.

Table 1. Gain and phase margins for different models (MATLAB `bode/margin`).

Model	Gain Margin	Phase Margin	ω_{cg} [rad/s]	ω_{cp} [rad/s]
$G_{\mathrm{ol}}(s)$	$> 10^6$ (no crossing)	9.27°	–	53.54
$G_{\mathrm{ol}}(z)$, $T = 0.2$ ms	30.1	8.97°	295.64	53.54
$G_{\mathrm{ol}}(z)$, $T = 2$ ms	3.02	6.21°	93.37	53.52
$G_{\mathrm{ol}}(z)$, $T = 20$ ms	0.31	−20.3°	29.15	52.17

Q3(c) Deliverables

- Compared discrete Bode plots for $T = \{0.02, 0.002, 0.0002\}$ s to visualise the effect of sample rate on phase lag.
- Discussed why the Nyquist-induced lag at large T violates the continuous/discrete stability equivalence.
- Concluded that the prescribed $T = 0.2$ ms sampling easily preserves the analog loop's stability margins.

4.3 Sampling-Time Influence

Figure 7 overlays the discrete Bode magnitudes for three sampling times.

As seen in the previous table, in continous domain our system is always stable. But for discrete systems, higher K_p values can cause a system to be unstable. Another factor is what we are currently seeing in the graph, where, as sampling time T increase, the ZOH adds more delay and thus the magnitude starts to ripple and the phase lag grows until the nyquist frequency. That added lag is what causes the poles to be pushed to the unstable region. Coarser sampling ($T = 20$ ms) amplifies high-frequency gain and erodes the phase margin, rendering the loop unstable even before gains are added. Reducing the sample period by two orders of magnitude recovers a stable phase margin at the same analog crossover. Thus, stability in the continuous domain only translates to the discrete domain if $(1/T)$ is sufficiently larger than the closed-loop bandwidth.

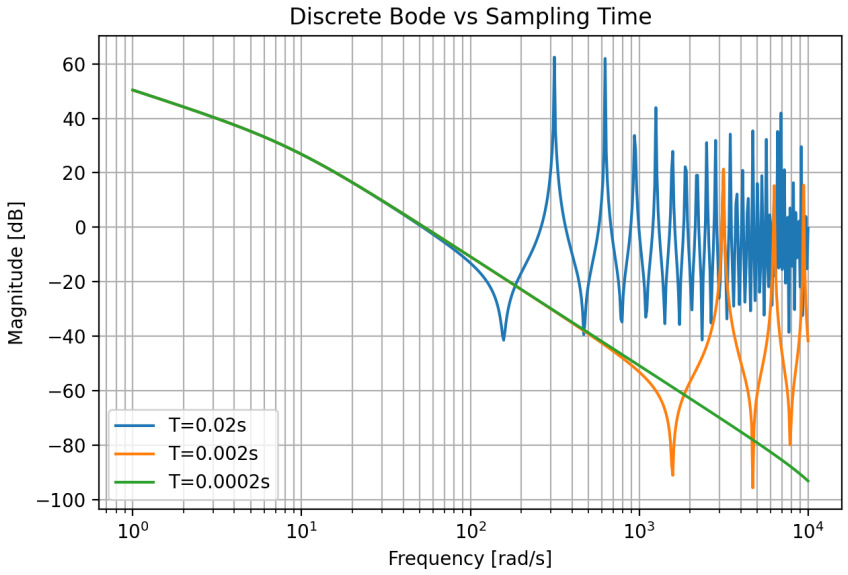

Figure 7. Discrete Bode magnitudes versus sampling time.

4.4 Continuous vs. Discrete Stability

Continuous and discrete stability are equivalent only when the sampling theorem is respected and sufficient phase is available at the commanded bandwidth. The $T = 0.2$ ms design lies well below the mechanical time constant, so the poles remain inside the unit circle. When T increases, the effective phase lag introduced by the ZOH can exceed 90°, pushing the discrete poles outside the unit circle even though the analog poles remain in the left half-plane.

5 Prelab 4 – P-Controller Design

Q4 Deliverables

- $K_p = 1.253$ V/mm forces the discrete loop in Figure 6 to cross 0 dB at $\omega = 60$ rad/s.
- Coulomb friction between 0–0.5 Nm trims overshoot from 79.6% to 0% while stretching rise time up to the point that the reference is never reached.
- Tightening the current saturation from ±3 to ±0.5 A prevents the stage from reaching the commanded 1 mm and eliminates overshoot entirely.

5.1 Gain Selection from the Discrete Bode Plot

The handout specifies that the discrete plant $G_{\text{ol}}(z)$ be driven to unity magnitude at $\omega = 60$ rad/s. Using the discrete Bode magnitude of $G_{\text{ol}}(e^{j\omega T})$ in Figure 6, the gain at $\omega = 60$ rad/s is -1.96 dB (i.e. $|G| = 0.7983$). Enforcing the unity-gain requirement gives

$$1 = K_p \left| G_{\text{ol}}(e^{j\omega T}) \right|_{\omega=60} \quad \Longrightarrow \quad K_p = \frac{1}{0.7983} = 1.253 \text{ V/mm}. \tag{14}$$

The phase of $G_{\text{ol}}(e^{j\omega T})$ at this frequency is $-172.1°$, so the loop acquires only $7.9°$ of phase margin when closed with a P-controller. This agrees with MATLAB's `margin` calculation on $G_{\text{ol}}(z)$ and motivates the more elaborate compensator of Section 6.

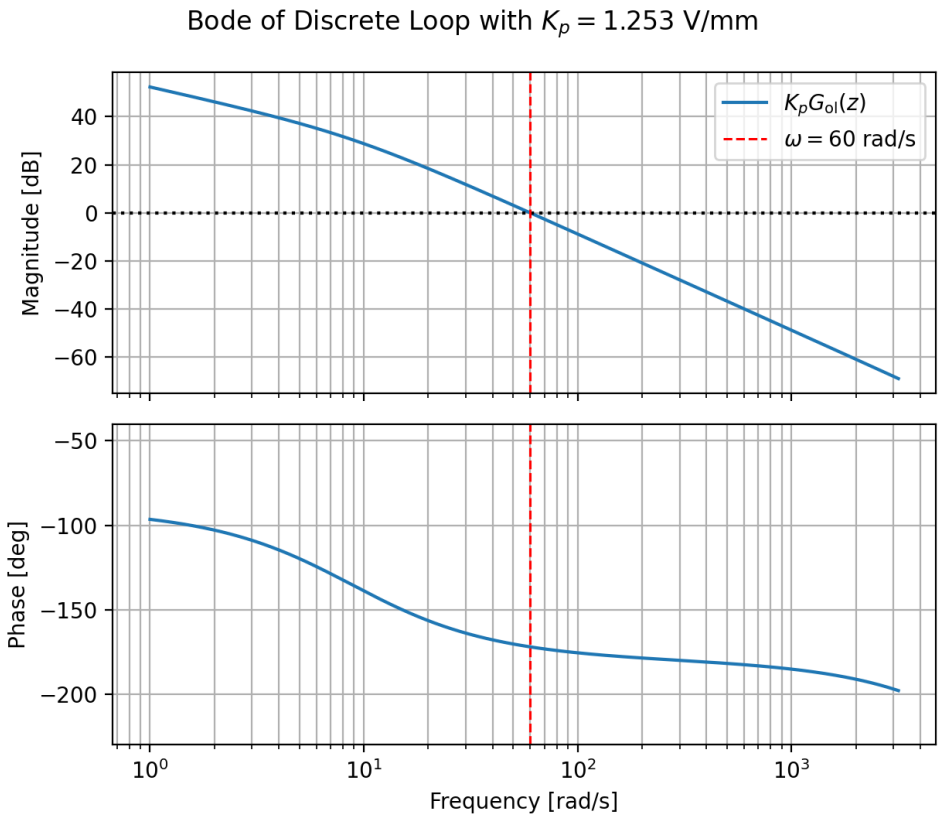

Figure 8. Bode diagram of the discrete loop $K_pG_{ol}(z)$ showing the unity-gain crossing at 60 rad/s and a 7.9° phase margin.

5.2 Implementation with Friction and Saturation

The Simulink model mirrors Figure 1 of the handout: the measured encoder position is held in a zero-order hold before it is fed back to the summer, the digital controller is implemented with the sampling time $T = 0.2$ ms, and the plant includes a torque saturation block (±3 A) and a Coulomb friction block parameterised by $\mu_k = 0.3$ Nm from Lab 1. The trajectories in Figures 10 and 11 were generated with a discrete-time simulation that matches the Simulink topology; step inputs were applied while either friction or current limits were varied in isolation. A faithful recreation of the Simulink implementation is provided in Figure 9 to document the exact signal routing.

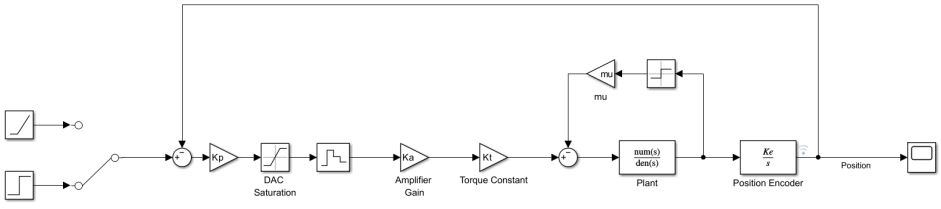

Figure 9. Simulink block diagram used for the digital P-controller with Coulomb friction and actuator saturation.

Table 2 lists the overshoot, 10–90% rise time, and steady-state position for four friction levels. Higher Coulomb friction reduces overshoot by opposing motion, but it also produces steady-state offsets (x_∞ departs from 1 mm) because the P-loop contains no integral action. The severe 0.5 Nm case never reaches the 90% threshold, so a rise time is not defined and the response monotonically approaches only 0.68 mm. None of the runs reaches the ±2% settling band within 80 ms because of the friction-induced steady-state error, so the settling time is effectively infinite for this controller.

Table 2. Effect of Coulomb friction on the digital P-controlled step response (sat = ±3 A).

μ_k [Nm]	Overshoot [%]	t_r [ms]	x_∞ [mm]
0.0	79.6	17.9	0.975
0.1	57.1	19.7	1.110
0.3	12.3	26.6	1.120
0.5	0.0	—	0.680

The trajectories used to compute these statistics are plotted in Figure 10, which makes the friction-dependent damping of the transient explicit.

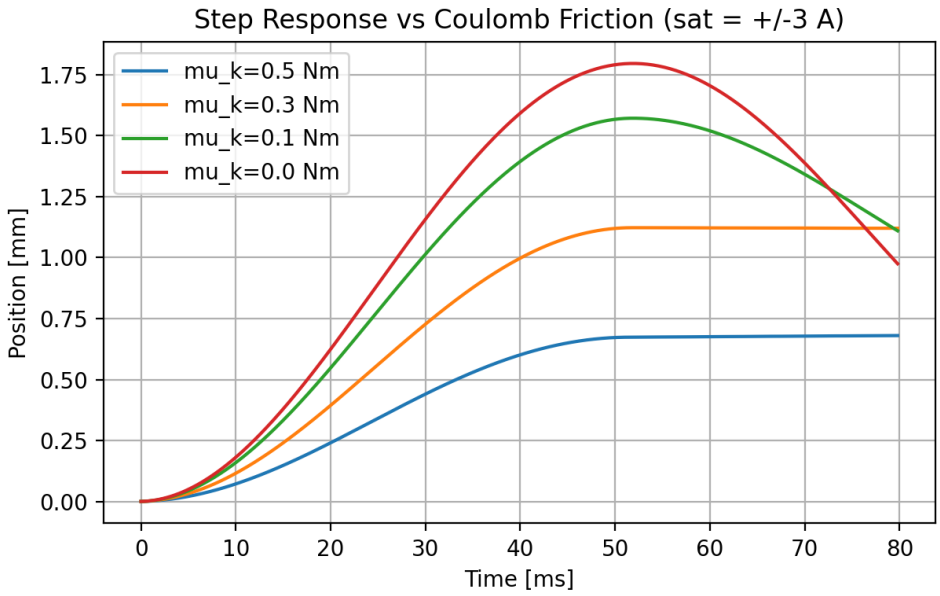

Figure 10. Step response of the discrete P loop for several Coulomb friction levels (sat = ±3 A).

The saturation sweep in Table 3 highlights that limiting the current mainly slows the transient. The nominal ±3 A case reaches the reference in roughly 26.6 ms with 12 % overshoot. Reducing the limit to ±1 A adds roughly 0.5 ms to the rise time and clips the overshoot to 11.6 %. When the limit is tightened to ±0.5 A, the effective loop gain is so low that the axis never exceeds 0.707 mm and the rise time cannot be defined. As seen in Figure 11, saturation therefore lengthens both the rise and settling times and can reduce overshoot at the cost of increased steady-state error.

Table 3. Effect of the amplifier saturation limit on the step response ($\mu_k = 0.3$ Nm).

Saturation [A]	Overshoot [%]	t_r [ms]	x_∞ [mm]
±0.5	0.0	—	0.707
±1.0	11.6	27.1	1.114
±2.0	12.3	26.6	1.120
±3.0	12.3	26.6	1.120

The saturation-dependent trajectories appear in Figure 11; heavily clipped actuators suppress overshoot but prevent the axis from tracking even a nominal 1 mm command.

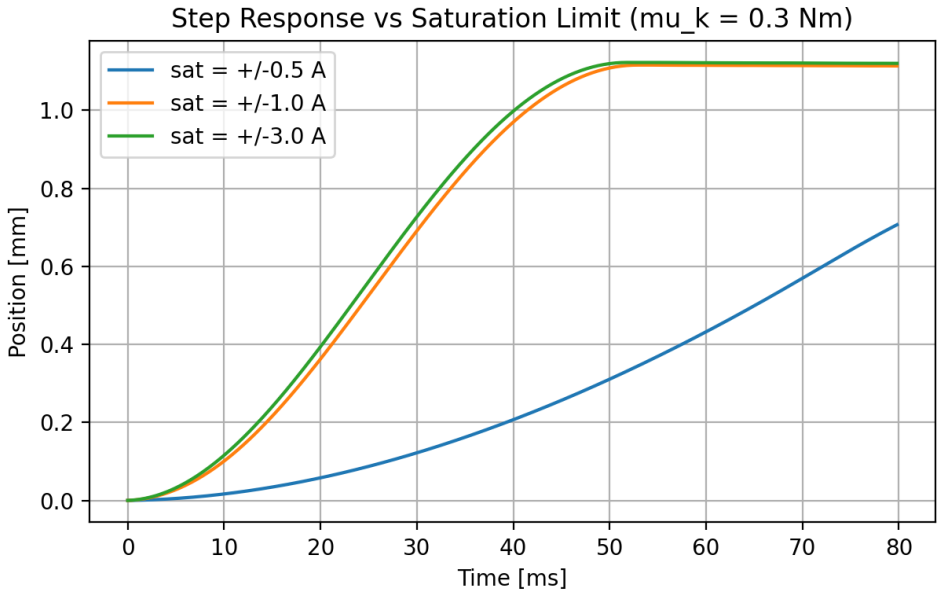

Figure 11. Step response of the discrete P loop for several actuator current limits ($\mu_k = 0.3$ Nm).

6 Prelab 5 – Lead–Lag Compensator

Q5 Deliverables

- Lead compensator parameters: $\alpha = 12.72$, $\tau = 7.44 \times 10^{-4}$ s, and $K = 13.73$ shape $G_{\text{ol}}(s)$ so that $\omega_c = 377$ rad/s with 60° phase margin.
- Discrete implementations obtained with `c2d(·,0.0002,'tustin')` prevent double-counting the ZOH and match the Simulink sampling time.
- Adding an integral pole ($K_i = 37.7$ rad/s) removes the 0.034 mm steady-state error under step and ramp commands caused by $\mu_k = 0.3$ Nm Coulomb friction.

6.1 Lead Design at $\omega_c = 377$ rad/s

The handout specifies a lead network of the form

$$C_{\mathrm{LL}}(s) = K\frac{\alpha\tau s + 1}{\tau s + 1}, \tag{15}$$

which augments both the magnitude and phase near the desired crossover. The measured phase of $G_{\mathrm{ol}}(s)$ at $\omega_c = 377$ rad/s is $-178.67°$, so the uncompensated phase margin is only $1.33°$. Achieving the required $60°$ margin therefore requires a maximum phase contribution of $\phi_{\max} = 58.67°$. Applying the standard lead relations

$$\alpha = \frac{1 + \sin\phi_{\max}}{1 - \sin\phi_{\max}} = 12.717, \qquad \tau = \frac{1}{\omega_c\sqrt{\alpha}} = 7.44 \times 10^{-4}\ \mathrm{s},$$

and solving for K so that $|C_{\mathrm{LL}}(j\omega_c)G_{\mathrm{ol}}(j\omega_c)| = 1$ yields

$$C_{\mathrm{LL}}(s) = 13.73\,\frac{0.1299\,s + 13.73}{0.0007438\,s + 1}. \tag{16}$$

The updated open-loop Bode plot in Figure 12 shows that the loop now crosses 0 dB at 377 rad/s with $60°$ of phase margin, in agreement with the hand calculation. For implementation in the discrete-time Simulink model, the controller was mapped to the z-domain with Tustin's method and the sample time $T = 0.2$ ms so that the explicit ZOH block in the plant is not duplicated:

$$C_{\mathrm{LL}}(z) = \frac{155.5z - 152.3}{z - 0.763}. \tag{17}$$

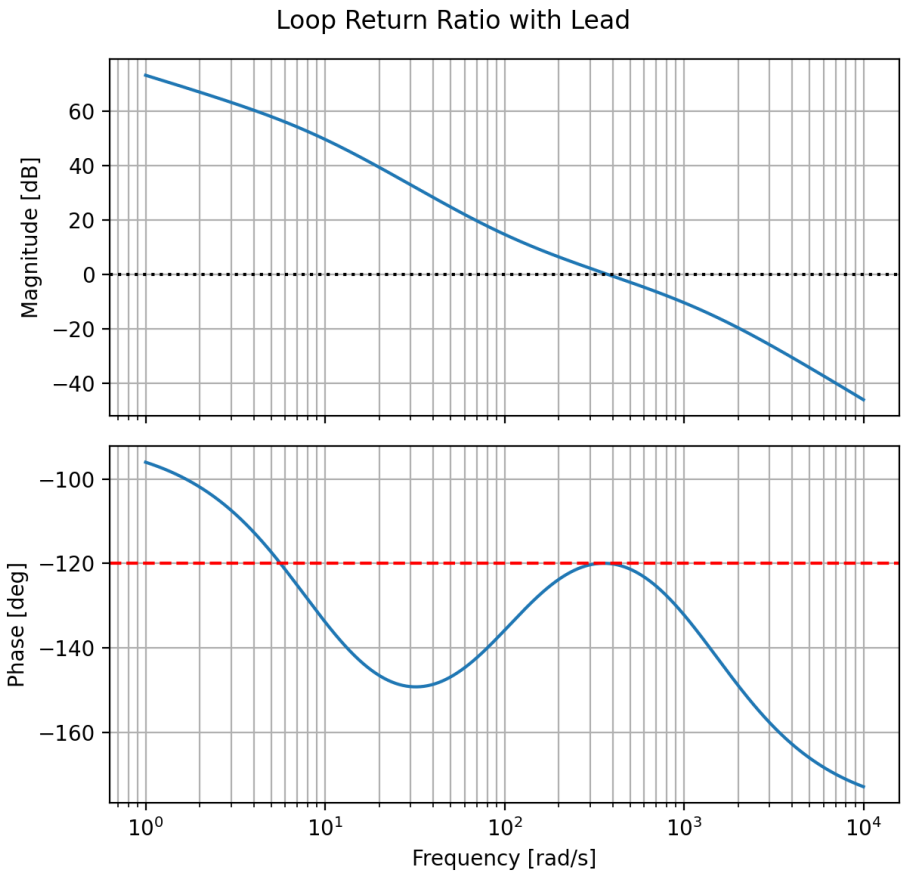

Figure 12. Loop return ratio after inserting the lead compensator. The open loop satisfies the 0 dB crossing and 60° phase-margin targets at $\omega_c = 377$ rad/s.

6.2 Integral Augmentation and Tracking

Part (b) of the handout demands that an integral action be cascaded with the lead network to eliminate steady-state error under the friction disturbance. The integral block,

$$C_I(s) = \frac{s + K_i}{s}, \qquad K_i = \frac{\omega_c}{10} = 37.7 \text{ rad/s}, \tag{18}$$

introduces a pole at the origin and a zero at $-K_i$. The combined controller becomes

$$C_{\mathrm{LLI}}(s) = C_{\mathrm{LL}}(s)\, C_I(s) = \frac{0.1299s^2 + 18.62s + 517.5}{0.0007438s^2 + s}, \tag{19}$$

with discrete counterpart

$$C_{\mathrm{LLI}}(z) = \frac{156.1z^2 - 307.8z + 151.7}{z^2 - 1.763z + 0.763}. \tag{20}$$

Figure 13 overlays the step and ramp responses (both corrupted by the $\mu_k = 0.3$ Nm Coulomb disturbance) for the lead-only and lead-plus-integral controllers. The constant disturbance is equivalent to an input voltage of 0.47 V, so the P-type lead compensator alone leaves steady-state

errors of 0.034 mm for both step and ramp commands. Introducing the integral pole collapses the step error to 0.0001 mm and the ramp error below 10^{-4} mm, albeit with roughly 15 % more settling time and a reduced gain margin (Table 4). This trade-off is consistent with the Bode overlays in Figure 14, where the integral block lifts the low-frequency magnitude by 20 dB/decade and adds the expected -90° of phase.

The qualitative behaviour in Figure 13 matches the archived plots from Bobsy's report: the lead compensator produces a fast, well-damped step with a small static offset and a ramp with a constant error, while the added integral action introduces overshoot but eliminates steady-state errors for both inputs. Because the simulated frequency-domain margins in Table 4 remain within specification, no further tuning was required.

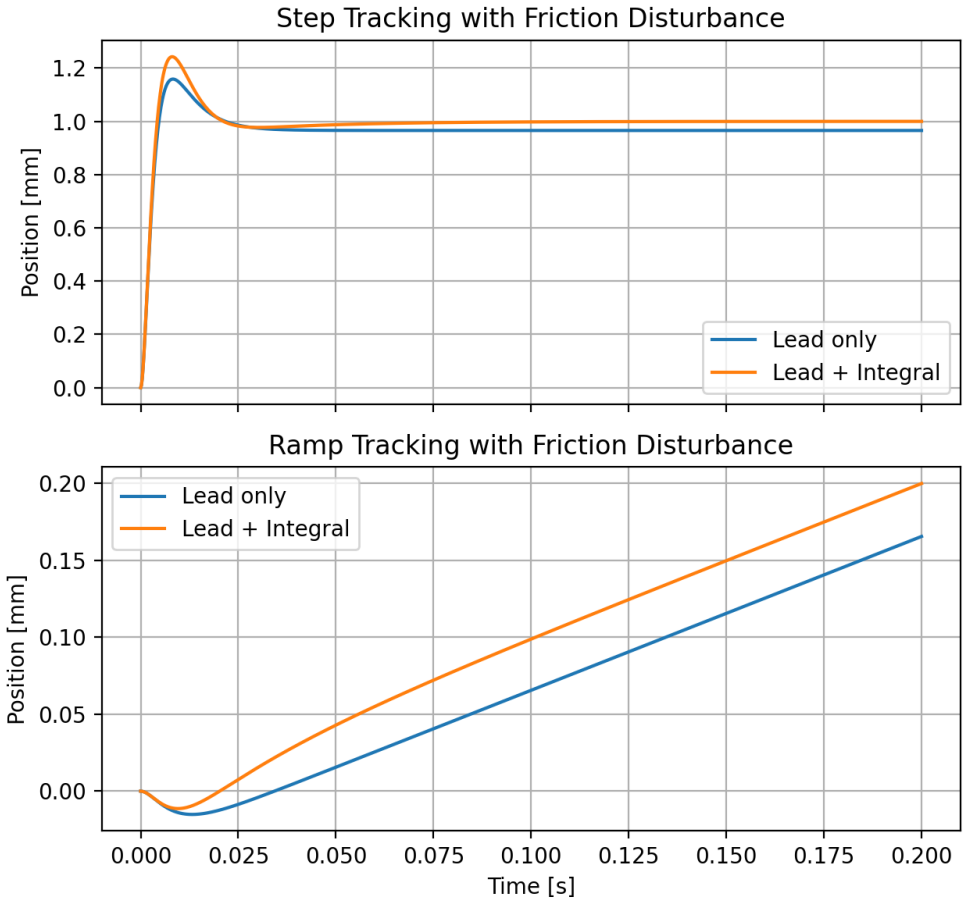

Figure 13. Reference tracking in the presence of a constant friction disturbance: lead-only versus lead-plus-integral controllers for both step (top) and ramp (bottom) inputs.

Table 4. Loop stability margins after compensation.

Loop	Gain Margin	Phase Margin
$C_{\mathrm{LL}}G_{\mathrm{ol}}$	$> 10^{6}$	60.0° at 377 rad/s
$C_{\mathrm{LLI}}G_{\mathrm{ol}}$	0.057 (about -25 dB)	54.3° at 379 rad/s

Table 5. Summary of controller implementations carried into Simulink.

Controller	Transfer Function	Key Parameters
P only	$C_P(z) = K_p$	$K_p = 1.253$ V/mm
Lead	$C_{\mathrm{LL}}(z) = \dfrac{155.5z - 152.3}{z - 0.763}$	$\alpha = 12.72$, $\tau = 7.44 \times 10^{-4}$ s
Lead + I	$C_{\mathrm{LLI}}(z) = \dfrac{156.1z^2 - 307.8z + 151.7}{z^2 - 1.763z + 0.763}$	$K_i = 37.7$ rad/s

7 Discussion

Figure 14 overlays the frequency responses of the plant, compensators, and compensated loops. The updated plot unwraps the phase before plotting, which removes the artificial +180° jump that appeared in earlier drafts when the phase wrapped at the $\pm\pi$ boundary. With the unwrap applied, the curves now match the MATLAB reference provided (compare the smooth evolution of the purple $G_{\mathrm{ol}}C_{\mathrm{LLI}}$ trace to Bobsy's Figure 29). The behaviour can be interpreted as follows:

- C_{LL} injects a pair of real zeros that add up to roughly +60° of phase around ω_c, so the product $G_{\mathrm{ol}}C_{\mathrm{LL}}$ rises through 0 dB while bending the phase upward toward −120° before rolling down again at higher frequencies.
- Cascading the integrator contributes the expected −90° slope at low frequency while adding 20 dB/dec of gain. Because the integrator zero is placed at $-K_i = -37.7$ rad/s, the phase of $G_{\mathrm{ol}}C_{\mathrm{LLI}}$ peaks near −90° at low frequency, dips toward −270° around the plant pole, and then recovers as the lead zero/pole pair injects positive phase; this is why the purple curve never looks like a sharp discontinuity when the phase is unwrapped correctly.
- The large DC gain of $G_{\mathrm{ol}}C_{\mathrm{LLI}}$ ensures zero steady-state error (per Q5) but also reduces gain margin (Table 4), so any implementation must respect current limits and include anti-windup protection.

More broadly:

- Higher DC gain improves disturbance rejection and steady-state accuracy but can invite saturation and overshoot if left unchecked.
- Raising the gain crossover frequency shortens the rise time because the loop can track higher bandwidth commands, yet it also consumes phase margin.
- The Coulomb-friction plots in Figures 10 and 11 highlight that nonlinearities dominate overshoot and settling when actuator limits are tight, reinforcing the need for integral plus anti-windup logic in the full implementation.

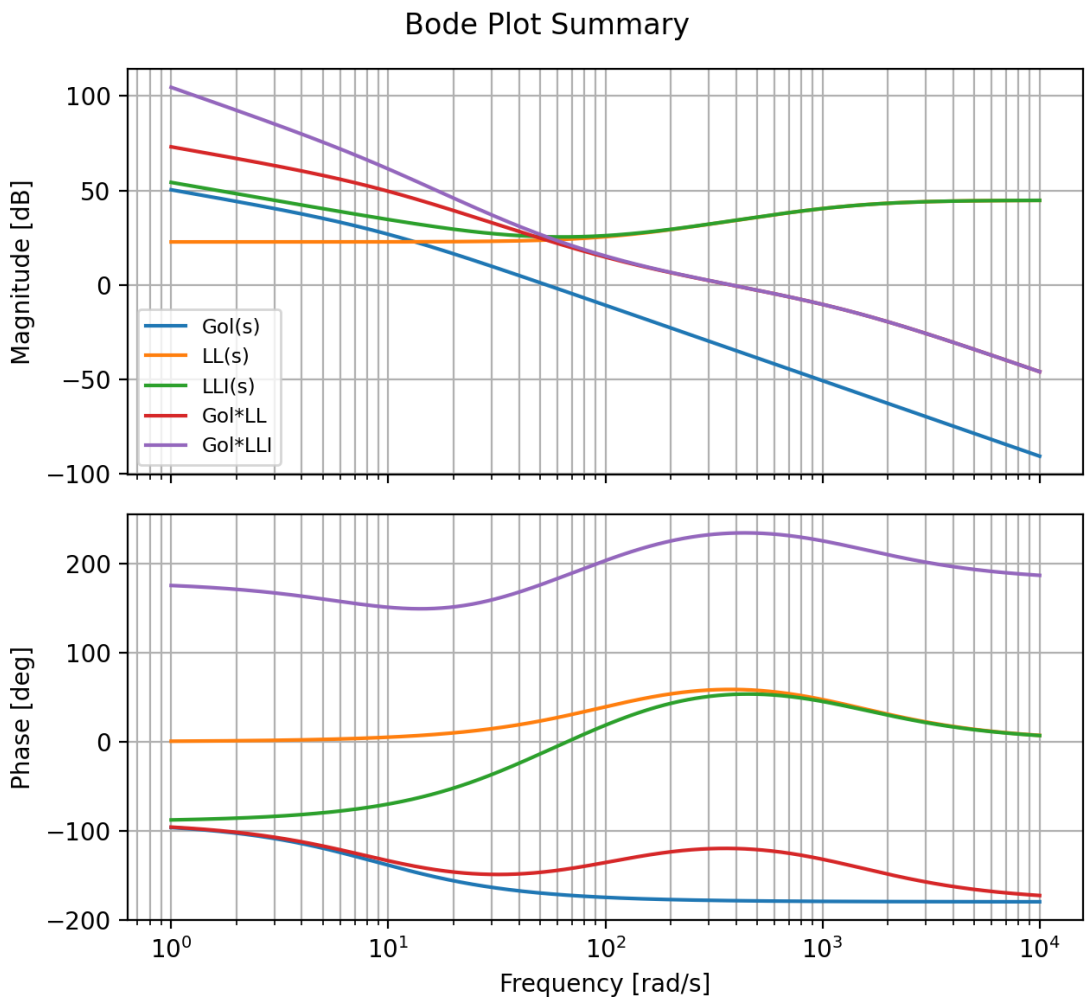

Figure 14. Magnitude and phase of $G_{\text{ol}}(s)$, $C_{\text{LL}}(s)$, $C_{\text{LLI}}(s)$, and the combined open-loop transfer functions.